Optical Materials 46 (2015) 168–174

Contents lists available at ScienceDirect

Optical Materials

journal homepage: www.elsevier.com/locate/optmat

Synthesis, characterization and luminescence studies in $ZrO_2:Dy^{3+}$ and $ZrO_2:Dy^{3+}$, Gd^{3+} films deposited by the Pyrosol method

R.C. Martínez-Olmos [a], J. Guzmán-Mendoza [a], A. Báez-Rodríguez [b], O. Álvarez-Fragoso [b], M. García-Hipólito [b,*], C. Falcony [c]

[a] Centro de Investigación de Ciencia Aplicada y Tecnología Avanzada, IPN, Unidad Legaria, Legaria #694, Col. Irrigación, Del. Miguel Hidalgo, C.P. 11500 México, D.F., Mexico
[b] Instituto de Investigaciones en Materiales, UNAM, Circuito Exterior, Cd. Universitaria, Coyoacán, 04510 México, D.F., Mexico
[c] Centro de Investigación y Estudios Avanzados del Instituto Politécnico Nacional, Apartado Postal 14-740, México, D.F. 07000, Mexico

ARTICLE INFO

Article history:
Received 20 December 2014
Received in revised form 15 March 2015
Accepted 1 April 2015
Available online 20 April 2015

Keywords:
Films
$ZrO_2:Dy^{3+}$
Pyrosol
Gd^{3+} codoping
White luminescence

ABSTRACT

ZrO_2, $ZrO_2:Dy^{3+}$ and $ZrO_2:Dy^{3+}$, Gd^{3+} films were synthesized using the Pyrosol technique. These films have a ZrO_2-metastable tetragonal crystalline structure, which is better defined as the deposition temperature increases. Photoluminescence and cathodoluminescence properties of these films were studied as a function of deposition parameters such as substrate temperature and Dy^{3+} and Gd^{3+} relative concentrations. All luminescent emission spectra showed the typical electronic transitions 4f → 4f of the Dy^{3+} ions at 480, 574 and 655 nm. The luminescent intensity is observed to increase with the Dy^{3+} ion concentration up to 7 at.% in the spraying solution (1.8 at.% inside films), higher concentration result in an inhibition of the luminescence. Incorporation of Gd^{3+} ions in $ZrO_2:Dy^{3+}$ films produced a marked increase in the luminescent emission intensity (approximately 15 times). The elemental composition and surface morphology of these films are also reported.

1. Introduction

The development of luminescent materials occupy a place of great importance in modern technology because of its use in many applications such as computer screens, signaling boards, some flat screens for television, electronic display panels, lighting and energy saving lamps. These devices incorporate luminescent materials in their design and for this purpose various materials are used as a host lattice (matrix) to accommodate the different ions which induce luminescence property [1,2]. The metallic oxides are very versatile materials which have physical and chemical properties that make them good candidates for use in the field of the optics, among them are their transparency in the ultraviolet–visible, high refractive index and a high fusion temperature, which makes them very stable in several ways. Among these metallic oxides, ZrO_2 is recognized for the high quality of its properties such as high resistance to corrosion, chemical and thermal stability, high mechanical strength, high refractive index, high-melting point and electrically insulating [3,4]. This oxide has also been used in fuel cells at high temperatures and in catalytic processes as oxygen sensor [5,6]. The ZrO_2 has a forbidden bandgap of 5.8 eV and has low phonon frequency (around 470 cm^{-1}) which allows its use as a host lattice for optically active ions that generate visible luminescence [7].

The optical properties of rare earth ions, considered as significant luminescence activators, have been the theme of diverse investigations in recent decades. Since its discovery, the research about its effects on crystalline and non-crystalline matrices has been intensified [1,8]. Several of these rare earth ions have been introduced into the ZrO_2 crystalline lattice to generate intensive visible light emission, examples of these are: ZrO_2:Eu [9,10], ZrO_2:Tb [11,12], ZrO_2:Pr [13,14], ZrO_2:Sm [15], ZrO_2:Er [16,17], ZrO_2:Nd [18], etc.

Dy^{3+} ion possess very interesting characteristics for white light generation; this ion incorporated in various matrices produce strong emission bands in the blue and yellow regions, which are typical of the 4f → 4f transitions. ZrO_2 matrix has proved its capability to hold Dy^{3+} ion to generate white light or near it. Related literature reports some studies on ZrO_2 powders optically activated with Dy^{3+} ions, most of which are synthesized at relatively high temperatures (800–1000 °C) [19–21]. To our best knowledge, the investigations about $ZrO_2:Dy^{3+}$ films are non-existent or scarce. Luminescent films, unlike those materials in powder form, exhibit advantages such as good adhesion to the substrate, unaltered

* Corresponding author. Tel.: +52 55 56224598; fax: +52 55 56161371.
E-mail addresses: rodmarolm@yahoo.com (R.C. Martínez-Olmos), joguzman@ipn.mx (J. Guzmán-Mendoza), adibr_1@hotmail.com (A. Báez-Rodríguez), oaf@unam.mx (O. Álvarez-Fragoso), maga@unam.mx (M. García-Hipólito), cfalcony@fis.cinvestav.mx (C. Falcony).

http://dx.doi.org/10.1016/j.optmat.2015.04.014
0925-3467/

properties throughout the covered area and better thermal stability [22]. The films, reported in this paper, were deposited at substrate temperatures $\leqslant$550 °C, which are considerably less than those used for the powder synthesis. There are various techniques for depositing materials in form of films such as: sputtering [23], sol–gel [24], Chemical Vapor Deposition (CVD) [25], Atomic Layer Deposition (ALD) [26], Liquid Phase Deposition (LPD) [27] and Pyrosol [28]. This last one has proved to be an effective technique for depositing thin and thick films and powders in a relatively simple and inexpensive process. This technique is able to produce a wide variety of materials, such as oxides, sulfides and selenides, from inorganic and metal–organic salts such as chlorides, nitrates, acetates and acetylacetonates [28].

This work reports the structural and optical properties of ZrO_2, ZrO_2:Dy^{3+} and ZrO_2:Dy^{3+}, Gd^{3+} films deposited by the Pyrosol technique. This study is focussed on the effect exerted by synthesis parameters such as deposition temperature and the doping concentration on the above-mentioned properties.

2. Experimental details

Undoped, Dy^{3+} and Dy^{3+}, Gd^{3+} doped ZrO_2 films were deposited by the Pyrosol technique. Roughly, this technique consists of generating (by ultrasonic means) a spray or aerosol from a precursor solution; this aerosol is carried to a heated substrate where a pyrolytic reaction is performed producing a solid film on the substrate. The deposition system is enclosed in an extraction chamber where residual reaction gases are removed. The precursor reagents used in this work were zirconium oxychloride ($ZrOCl_2{\cdot}8H_2O$), dysprosium trichloride ($DyCl_3{\cdot}6H_2O$) and gadolinium trichloride ($GdCl_3{\cdot}6H_2O$) all from Aldrich Chemicals Co., with a purity of 99.99%. Deionized water was used as solvent (with a resistivity of 18 MΩ/cm). The substrates were 1 cm × 1.5 cm "Corning" glass slabs and silicon wafers of the same dimensions. The samples deposited on silicon substrates were used only for elemental chemical composition measurements by Energy Dispersive Spectroscopy (EDS). The chemical reaction that gives origin to the ZrO_2 films is

$$ZrOCl_2 + H_2O \rightarrow ZrO_2 \downarrow + 2HCl \uparrow$$

where the down arrow indicates a solid product (film on the substrate) and the up arrow indicates the residual material that escapes in gaseous form. Deposition temperatures were varied from 400 °C to 550 °C, in 50 °C steps. Doping concentrations of the luminescence activators (Dy and Gd) were varied as follows: 0, 1, 3, 5, 7, 10, 15 and 20 at.% (atomic percent) for dysprosium and 0, 0.5, 1, 3, 5 and 10 at.% for gadolinium, measured with respect to the zirconium content. Some parameters that were kept constant during the deposits were: molarity of the solutions (0.5 M), deposition time (5–6 min), the carrier gas flow (dry air, 10 l per minute) and frequency of the ultrasonic generator (1.6 MHz).

The crystalline structure of the deposited films was determined with a X-ray Diffractometer (XRD), Siemens, model D-5000; the surface morphology with a Scanning Electron Microscope (SEM) JEOL, model JSM-6390LV; the chemical composition by EDS using a Si–Li detector brand Pentafet Oxford, installed in the previously-mentioned SEM; the Photoluminescence emission (PL) using a spectrofluorometer model FluoroMax-P, JobinYvon Horiba and Cathodoluminescence (CL) measures were carried out in a steel vacuum chamber equipped with an cold cathode electron source Luminoscope, model MCA-2 ELM, RELION Co.; the samples are placed inside the above-mentioned chamber and evacuated to a pressure $\leqslant 10^{-3}$ Torr. The electron beam is produced parallel to the sample surface and is deflected 90°, by a magnetic field, to make it impact perpendicular to the surface of the films. The visible light emitted from the samples is carried by an optical fiber, to the aforementioned spectrofluorimeter to record the CL spectra. The current value was 0.03 mA and the area of the incident beam on the surface of the films was 0.07 cm^2. The films thickness was about 5 μm as measured with a profilometer Sloan Dektak IIA with an uncertainty of ±0.3 μm.

3. Results and discussion

Fig. 1 shows the X-ray diffractograms obtained for ZrO_2 films depending on deposition temperatures. The films deposited at temperatures from 400 °C to 450 °C, have an amorphous or non-crystalline structure. Whereas those films deposited at 500 °C and 550 °C show narrower and intense peaks, indicating that there is an increase in the size of the crystallite constituents of the films. The observed crystalline structure corresponds to the meta-stable tetragonal phase of ZrO_2 according to the diffraction letter ICSD 066783. The peaks centered at 30.1°, 35.3°, 50.0°, 60.2° and 62.8° are assigned to the crystallographic planes (101), (110), (112), (211) and (202), respectively. It is appreciated that the peak corresponding to (101) plane is the most intense.

In the synthesis of the ZrO_2 films whose substrate temperatures are lower than 450 °C, the thermal energy at low substrate temperatures causes a low mobility of the reactive ions, which limits the growth kinetics during the deposition process giving rise to partially crystallized material coexisting with amorphous regions. As the deposition temperature increases (temperatures higher than 450 °C), the thermal energy available now allows the formation of crystallites, which is manifested in relatively intense peaks in the X-ray diffractograms. By using the Scherrer formula an estimate of the size of the constituent crystallites for the films deposited at 550 °C was 30 nm. For this purpose, data of the peak centered at $2\theta = 30.1°$ were considered.

Fig. 2 shows micrographs, obtained by SEM, from the surface of the ZrO_2 films. The films deposited at 400 °C and 450 °C show the formation of a branched rough surface with cracks, pores and the presence of some spherical particles which is a characteristic of a not completely processed material due to the low thermal energy involved at these deposition temperatures as mentioned above. The surface morphology of the films deposited at 500 °C and 550 °C presents less porosity because the pyrolytic reaction is favored with increasing thermal energy on the substrate surface. In general, the films exhibit a surface morphology with a homogeneous distribution of the deposited material, with full coverage over the entire surface of the substrate and with good adhesion thereto.

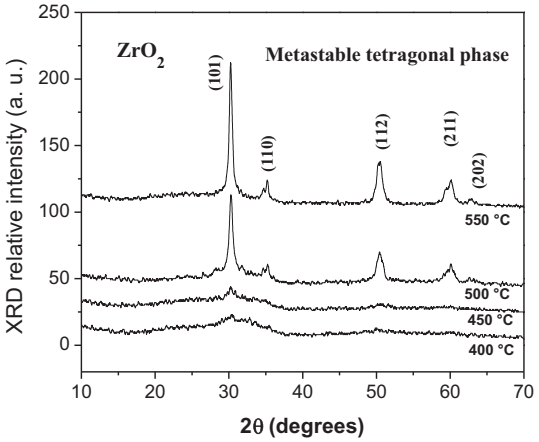

Fig. 1. Diffractograms for ZrO_2 films, as a function of the substrate temperatures.

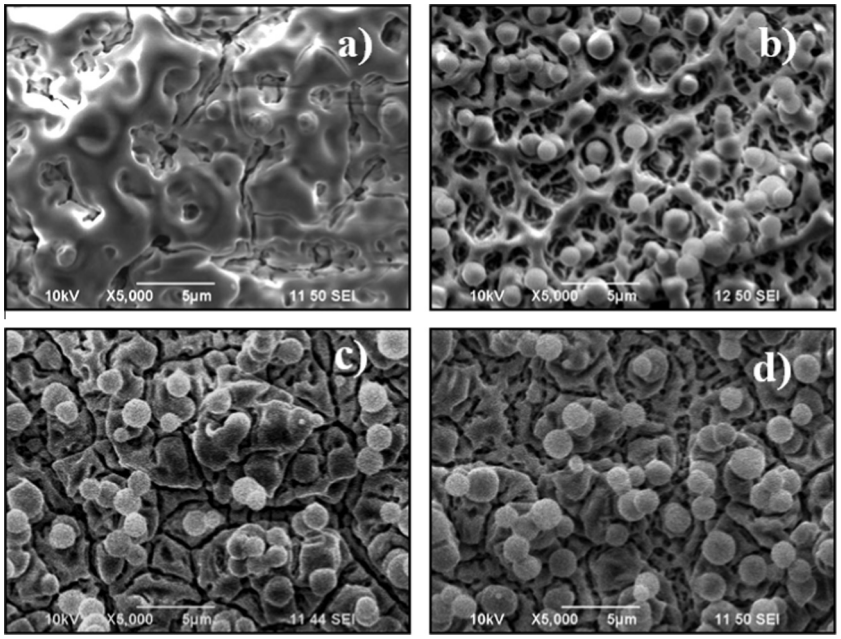

Fig. 2. SEM micrographs of ZrO_2 films, for different deposition temperatures (a) 400, (b) 450, (c) 500 and (d) 550 °C.

Tables 1 and 2 list the relative atomic percentage of each element present into the ZrO_2:Dy^{3+} films, as measured by EDS. Table 1 shows the elemental composition of the ZrO_2:Dy^{3+} films deposited with different $DyCl_3$ content in the precursor solutions; the substrate temperature during deposition was kept fixed at 550 °C. The amount of Dy that remains in the film is about 25–30% of the Dy content in the spraying solution. Also the amount of chlorine in the film is proportional to the $DyCl_3$ content in the spraying solution, reaching up to 7 at.% for films deposited with 20% $DyCl_3$ in the spraying solution, suggesting that this chlorine remaining in the film is somehow associated with the Dy incorporation. Since the relative content of the elements analyzed is normalized to sum 100%, the observed reduction of the Zr and O contents is partly explained when the amount of $DyCl_3$ is added.

Table 1
Atomic percent of the oxygen, zirconium, dysprosium and chlorine in the ZrO_2:Dy^{3+} films as measured by EDS for different $DyCl_3$ concentrations in the spraying solution. The substrate temperature was 550 °C.

$DyCl_3$ concentration in the deposition solution (at.%)	Oxygen (at.%)	Zirconium (at.%)	Dy (at.%)	Chlorine (at.%)
1	66.0	32.9	00.3	00.8
3	65.7	32.0	00.7	01.6
5	64.1	31.8	01.4	02.7
7	63.9	31.9	01.8	02.4
10	62.0	30.5	02.7	04.8
15	62.1	28.4	03.1	06.4
20	61.6	26.9	04.5	07.0

Table 2
Atomic percent of the oxygen, zirconium, dysprosium and chlorine in the ZrO_2:Dy^{3+} films as determined by EDS for different deposition temperatures. In this case, the $DyCl_3$ concentration in the start solution was 7 at.%.

Deposition temperature (°C)	Oxygen (at.%)	Zirconium (at.%)	Dy (at.%)	Chlorine (at.%)
400	60.9	29.6	03.2	06.3
450	61.6	30.8	02.7	04.9
500	62.7	31.7	02.1	03.5
550	63.9	31.9	01.8	02.4

However, the Zr/O ratio reduction from ~0.5 to 0.44 (for samples with 1–20 at.% of $DyCl_3$) indicates that, at least partially, Dy and Cl replace some Zr atoms in the ZrO_2 network. The issue concerning charge neutrality is not well determined, since the exact way that the Dy–Cl atoms are incorporated is not clear, neither if additional impurities like H and/or intrinsec defects might play a role. Table 2 displays the results on the elemental chemical composition of the ZrO_2:Dy^{3+} films as a function of the substrate temperature during deposition; the $DyCl_3$ content is maintained constant in the starting solutions (7 at.%). In this case, it is possible to see that low deposition temperatures favor the incorporation of dysprosium and chlorine in the film. As the substrate temperature increases, the thermal energy available dissociates the $DyCl_3$ molecules more efficiently as the Cl/Dy ratio indicates (~2 at 400 °C to 1.3 at 550 °C), thus, it is likely that the chlorine is incorporated in the film in an associated form with the Dy atoms [19]. In general, increasing deposition temperature results in a better stoichiometric composition.

Fig. 3 shows the PL excitation spectrum for ZrO_2:Dy^{3+} (7 at.%) films deposited at 550 °C. This spectrum shows a prominent broad

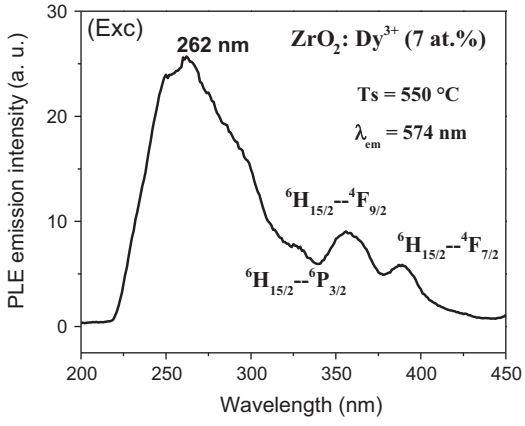

Fig. 3. Excitation spectrum for ZrO_2:Dy^{3+} (7 at.%) films. The deposition temperature was 550 °C and the emission wavelength was fixed at 574 nm.

band centered at 262 nm which produces the highest PL emission intensity when the emission wavelength is fixed at 574 nm. This broad band could be associated with absorptions due to charge transfer, in a similar way as reported for other hosts like Y_2O_3, La_2O_3 and YPO_4 [29–31]. Also, the spectrum exhibits lower intensity peaks centered on 327 nm, 354 nm and 388 nm, which correspond to the transitions ($^6H_{15/2} \rightarrow {}^6P_{3/2}$), ($^6H_{15/2} \rightarrow {}^4F_{9/2}$) and ($^6H_{15/2} \rightarrow {}^4F_{7/2}$), respectively, typical of the Dy^{3+} ions. From this spectrum, the wavelength of 262 nm is chosen to excite the samples studied in this work.

Fig. 4 shows the PL emission spectra for ZrO_2:Dy^{3+} films deposited at 550 °C, with doping concentration in the precursor solution from 0 to 20 at.%. These films were excited with a wavelength of 262 nm. The spectra show bands centered at 480 nm, 574 nm and 655 nm, owing to electronic transitions: $^4F_{9/2} \rightarrow {}^6H_{15/2}$, $^4F_{9/2} \rightarrow {}^6H_{13/2}$ and $^4F_{9/2} \rightarrow {}^6H_{11/2}$ characteristic of Dy^{3+} ions. It is observed that the yellow band (574 nm) is the most intense. As the doping concentration increases, an increasing PL intensity is observed, the greater intensity of the PL emission is obtained in films activated with 1.8 at.% inside the films. Higher concentrations of Dy^{3+} ions incorporated into the matrix cause a PL inhibition. The PL inhibition could have various origins; one of them is that the PL intensity quenching might occur because higher dopant concentrations give place to shorter average distances between Dy^{3+} ions in such way that energy transference among them starts to take place, increasing the probability of getting into a non radiative energy sink like a host lattice defect (concentration quenching). However this is only one possibility and it cannot exclude other possibilities; for example, in this case, the chlorine ions incorporated in large concentrations could reduce the energy transfer efficiency. Moreover, there is a broad band centered at approximately 435 nm originated at the ZrO_2 matrix that appears in all spectra of Fig. 4, the emission peaks associated with the Dy^{3+} ions are superimposed on this band. As the doping concentration increases the contribution of the 435 nm broad band decreases in intensity, but also does the Dy^{3+} ions related emission.

PL emission spectra for ZrO_2:Dy^{3+} (7 at.%) films as a function of the deposition temperature and excited with 262 nm radiation are shown in Fig. 5, where the typical emissions for Dy^{3+} ion are observed. The films with greater PL emission intensity are those deposited at 550 °C. This behavior could be a result the better crystalline quality of the films obtained as the deposition temperature is increased (Fig. 1), which allows for the incorporation of the Dy^{3+} ions into a less chaotic local environment inside the films.

Fig. 6 presents the behavior of the CL emission intensity for the peak centered at 574 nm in the spectra for ZrO_2:Dy^{3+} films, as a function of the activator ions concentration. For these films the deposition temperature was 550 °C and the acceleration voltage of the incident electrons was 8 kV. The inset exhibits the spectrum with the best emission intensity (curve b) and a CL spectrum of a pure ZrO_2 film (curve a: in this case no emission peaks are observed). As in the case of the PL (see Fig. 4), these spectra exhibit bands centered at 480 nm, 574 nm and 655 nm, corresponding to electronic transitions: $^4F_{9/2} \rightarrow {}^6H_{15/2}$, $^4F_{9/2} \rightarrow {}^6H_{13/2}$ and $^4F_{9/2} \rightarrow {}^6H_{11/2}$ owing to Dy^{3+} ions. It is also appreciated that the dominant emission peak is that at 574 nm. It can be observed that the highest CL emission intensity is obtained for films doped with 7 at.% of $DyCl_3$ in the precursor solution (1.8 at.% Dy incorporated inside films). Larger amounts of Dy^{3+} ions induce an inhibition of the CL emission intensity. Interestingly, the CL spectra do not show the broad band emission at 435 nm from the host lattice, as in the case of the PL (see Fig. 4). Also, unlike PL spectra, in the case of the CL spectra, a splitting of the blue band centered at 480 nm is appreciated; which becomes more pronounced for 3, 5 and 7 at.% doping concentrations. It is well known that levels of trivalent rare earth ions, in a crystalline environment, undergo the influence of asymmetric electric fields, generally produced by impurities and/or crystalline defects [32]. The band centered at 480 nm is due to a magnetic dipole transition whose intensity is less influenced by the environment in which is immersed the ion, unlike the one

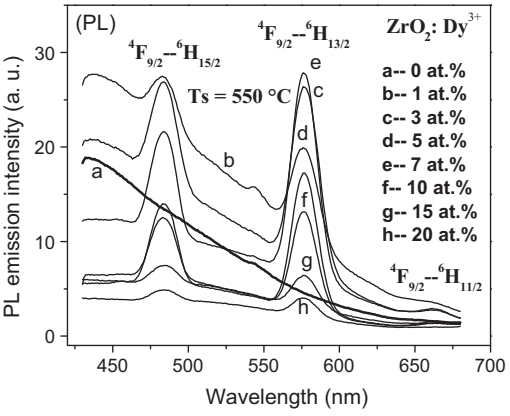

Fig. 4. PL emission spectra for ZrO_2:Dy^{3+} films deposited at 550 °C, as a function of the activator concentration (Dy^{3+}). The excitation wavelength was 262 nm.

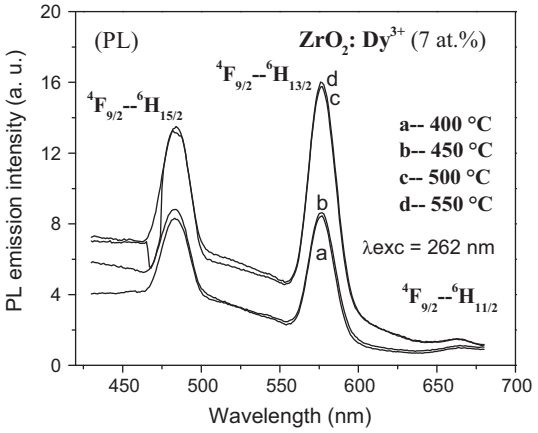

Fig. 5. PL emission spectra for ZrO_2:Dy^{3+} (7 at.%) films, with variations in the values of the deposition temperature. The excitation wavelength was 262 nm.

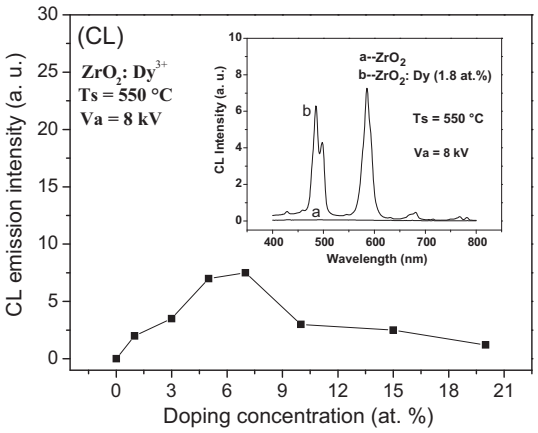

Fig. 6. Behavior of the CL emission intensity of the peak centered at 574 nm in the spectra for ZrO_2:Dy^{3+} films, deposited at 550 °C, depending on the activator concentration (Dy^{3+}). The electron accelerating voltage was 8 kV. The inset shows (a) CL spectrum of a pure ZrO_2 film and (b) CL spectrum for a ZrO_2:Dy^{3+} (1.8 at.%) film.

centered at 574 nm which is due to an electric dipole transition whose intensity is very dependent of the crystal field acting on the Dy^{3+} ions. The nature of the observed splitting in the CL spectra of the films under study in this work is unclear and further study is necessary. It should be considered that the PL emission may strongly depend on the excitation energy $h\nu$, which can be used for selective excitation of particular emission processes, i.e. a selective excitation of the activator ions in the host lattice may be achieved by using selected exciting wavelengths. The photon energy, in this case, is about few eV. In contrast with PL, CL always contains the luminescence from the activator ions excited directly and indirectly by the incident electrons; in this case all the available luminescence mechanisms are present to one degree or another in the excited material. CL is a very complex phenomenon, in which the electrons beam interacting with the solid sample generates many other phenomena, such as secondary electron emission, X-rays and Auger electron all having the possibility to contribute in one way or another to the observed emission. In this case, the electron energies involved are of the order of kV [33,2].

Fig. 7 shows the variation corresponding to the CL emission intensity of the band centered at 574 nm for ZrO_2:Dy^{3+} (7 at.%) films, as a function of the deposition temperature. The accelerating voltage of the exciting electrons was 8 kV. Again, as in the case of the PL spectra, typical emissions from Dy^{3+} ions with more intense yellow band are observed. Splitting of the blue band was also appreciated in the samples mainly deposited at the higher temperatures. The higher CL emission intensity is obtained for samples deposited at the highest deposition temperature used (550 °C), similar to the case of the PL spectra. Changes in the CL emission intensity for the yellow band of the films under study, but now as a function of the electron accelerating voltage (V_a) can be seen in the inset of Fig. 7. Here the films were deposited at 550 °C and the concentration of activator ions was 7 at.% into the precursor solution. The V_a values were 4, 6, 8 and 10 kV. The inset clearly shows that at higher V_a applied, CL emission intensity is greater. As the V_a increases the penetration of the electrons in the body of the film is deeper and therefore larger is the volume of excited Dy^{3+} ions which naturally produces superior emission intensity. By using a $V_a \geqslant 10$ kV some damage is observed on the films surface (due to the high kinetic energy of the incident electrons) for this reason a value of 8 kV was chosen to excite the films deposited as a function of the doping concentration and substrate temperature.

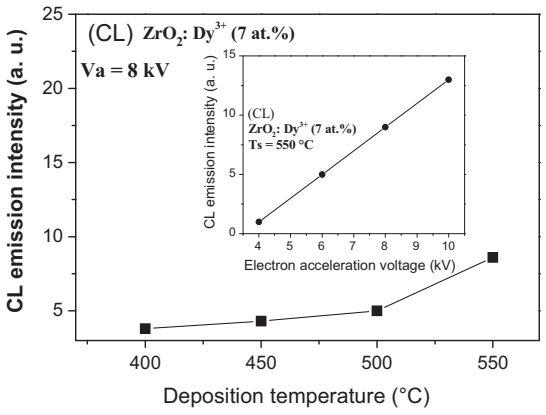

Fig. 7. Variation of the CL emission intensity for the band centered at 574 nm in ZrO_2:Dy^{3+} (7 at.%) films, as a function of the deposition temperature. The electron accelerating voltage was 8 kV. The inset shows changes in the CL emission intensity for the yellow band (574 nm) in ZrO_2:Dy^{3+} (7 at.%) films deposited at 550 °C, as a function of the electron accelerating voltage (V_a).

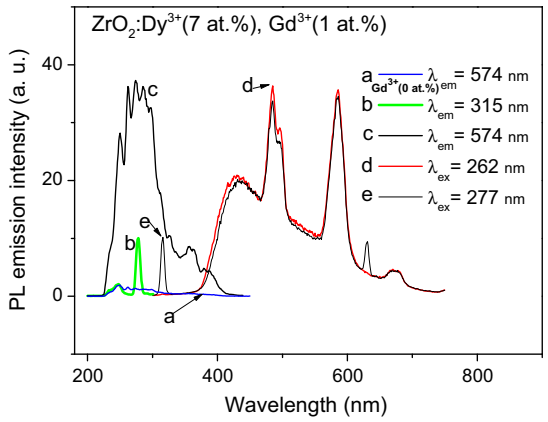

Fig. 8. Excitation and emission spectra from a ZrO_2:Dy^{3+}, Gd^{3+} film, deposited at 550 °C. The concentration of Dy^{3+} ions was fixed at 7 at.% and Gd^{3+} ions at 1 at.%. Also, it is appreciated a excitation spectrum from ZrO_2:Dy^{3+} (7 at.%) film recorded fixing the emission at 574 nm.

Fig. 8 shows excitation and emission spectra from a ZrO_2:Dy^{3+}, Gd^{3+} film, deposited at 550 °C. The concentration of Dy^{3+} ions was fixed at 7 at.% and Gd^{3+} ions at 1 at.%. Also, it is appreciated a excitation spectrum from ZrO_2:Dy^{3+} (7 at.%) film recorded fixing the emission at 574 nm (curve a). The excitation spectra for ZrO_2:Dy^{3+}, Gd^{3+} films were measured fixing the emissions at 315 nm (curve b) and 574 nm (curve c). Curve b shows two bands centered at 250 nm and 277 nm which correspond to $^8S_{7/2} \rightarrow {}^6D_{9/2}$ and $^8S_{7/2} \rightarrow {}^6I_{9/2}$ electronic transitions in Gd^{3+}, respectively (this indicates that 277 nm is the optimal wavelength to excite Gd^{3+} ions). The spectrum in curve c exhibits a prominent broad band with superimposed peaks centered at 250, 262, 373, 285 and 296 nm. Absorption bands of f–f transitions of Dy^{3+} ions are observed as small peaks at longer wavelengths. As it was already previously established the peak around 262 nm is attributed to charge transfer process from O^{2-} ion to Dy^{3+} (Dy–O) [34]. Here it is convenient to notice that the peaks on curve b coincide in wavelength with some peaks on curve c. The presence of Gd^{3+} transitions lines in the excitation spectrum of ZrO_2:Dy^{3+}, Gd^{3+} films (curve c) while monitoring the 574 nm emission of Dy^{3+} ions points out Gd^{3+} to Dy^{3+} energy-transfer [35]. In addition, it is observed from the excitation spectrum for ZrO_2:Dy^{3+}, Gd^{3+} films (curve c) that the intensity of the broad band is higher than the Gd^{3+} free sample (curve a). The increase of intensity in 220–300 nm regions with the incorporation of Gd^{3+} ions indicates an energy transfer from Gd^{3+} to Dy^{3+} by possible processes as those described by Singh et al. [36]. However, the interpretation for the improvement of luminescence properties of a RE^{3+}-doped host lattices after co-doping with Gd^{3+} ions is still not reasonably understood. Diverse energy-transfer mechanisms have been proposed by other authors [37–39]. It is likely that the presence of the Gd^{3+} ions in this matrix increases the luminescence properties of Dy^{3+}-doped ZrO_2 films because Gd^{3+} ions have better matching energy levels to accept the energy from the ZrO_2 host and subsequently pass it on to the Dy^{3+} ions. Also, the increase of the emission intensity could be due to the change of local crystal field of the Dy^{3+} ions after the co-doping of Gd^{3+} ions into the ZrO_2 host lattice [37]. Fig. 8 also shows the emission spectra from ZrO_2:Dy^{3+}, Gd^{3+} films excited with 262 m (curve d) and excited with 277 nm (curve e). In the curve d the typical electronic transitions from Dy^{3+} ions are observed, but the transitions associated with Gd^{3+} ions are not visible. The excitation with 277 nm exhibits a band centered at 315 nm associated to $^6P_{7/2} \rightarrow {}^8S_{7/2}$ transition from Gd^{3+} ions, besides the characteristic emissions from Dy^{3+} ions are appreciated (it is also visible a band centered at 630 nm which is associated to

the second harmonic of that centered at 315 nm). It is remarkable that the blue and yellow bands associated to Dy^{3+} ions have practically the same emission intensity in both cases; i.e. the samples excited with 262 nm and 277 nm are nearly the same spectra (except for the bands associated to Gd^{3+} ions).

Fig. 9 displays the PL spectra for ZrO_2:Dy^{3+}, Gd^{3+} films as a function of the atomic percent of Gd^{3+} ions in the spraying solution, the films were deposited at 550 °C, the concentration of Dy^{3+} ions was fixed at 7 at.% in the spraying solution and the excitation wavelength was 262 nm. The PL emission intensity increases with the addition of Gd^{3+} ions up to 1 at.%, higher values result in a quenching behavior of the PL emission intensity, even though the films with Gd^{3+} ions presented always a larger intensity than those without this co-dopant. The intensity of the band centered at 574 nm is about 15 times stronger in the film with 1 at.% of Gd^{3+} ions (curve a) than that of the film without Gd^{3+} ions (curve f). This notable result is explained by the arguments given in the discussion for Fig. 8.

The CL spectra for ZrO_2:Dy^{3+}, Gd^{3+} films as a function of the atomic percent of Gd^{3+} ions are shown in Fig. 10, for films deposited at 550 °C and the concentration of Dy^{3+} ions was set at 7 at.% in the starting solution. In this case, the observed results are similar to those presented in Fig. 9 for PL, except that the most intense CL emission corresponds to 3 at.% Gd^{3+} ions in the spraying solution. In general, the doping concentrations values for optimal

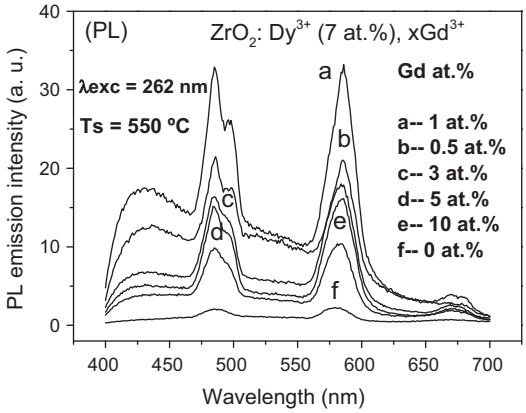

Fig. 9. PL emission spectra for ZrO_2:Dy^{3+}, Gd^{3+} films, with variations in the atomic percent of Gd^{3+} ions and excited with 262 nm. Studied films were deposited at 550 °C and the concentration of Dy^{3+} ions was fixed at 7 at.% in the precursor solution.

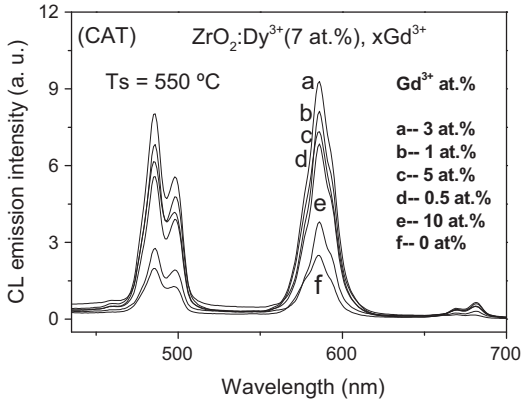

Fig. 10. CL emission spectra for ZrO_2:Dy^{3+}, Gd^{3+} films, with variations in the atomic percent of Gd^{3+} ions. The used V_a was 8 kV. These films were deposited at 550 °C and the concentration of Dy^{3+} ions was fixed at 7 at.% in the precursor solution.

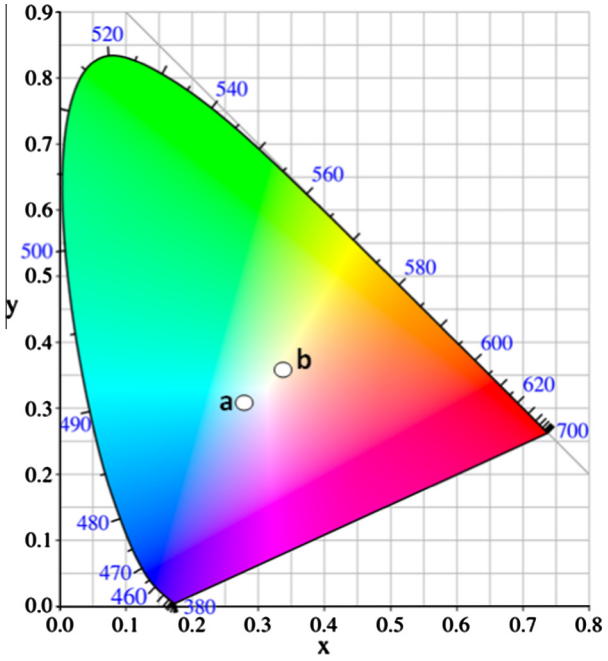

Fig. 11. Chromaticity diagram for ZrO_2:Dy^{3+} (7 at.%), Gd^{3+}(1 at.%) film (point a) and ZrO_2:Dy^{3+} (7 at.%) film (point b); both deposited at 550 °C and excited with 262 nm.

emission intensity do not always are the same in PL and CL, since the excitations with photons or with accelerated electrons are of different nature and they can reach their maximum emission intensity with different values of the impurity in question [29].

Fig. 11 shows a diagram of chromaticity coordinates, CIE (Commission Internationale de l'Eclairage, 1931), one of the points (a) correspond to the spectrum of the ZrO_2:Dy^{3+} (7 at.%), Gd^{3+} (1 at.%) film and the other one (b) to the spectrum corresponding to ZrO_2:Dy^{3+} (7 at.%) film. Since the main emissions from Dy^{3+} ions are located in the blue and yellow regions it is possible to generate white light emission when the intensities of these emissions have a proper balance relationship. The point (a) has coordinates (0.3085, 0.3102) falling in the bluish-white light region. The point (b) is situated at the yellowish-white region, whose coordinates are (0.3637, 0.3628); which are close to ideal ones for white color coordinates (0.3333, 0.3333). Then the films studied in this work are promising candidates for generating white light.

4. Conclusions

ZrO_2, ZrO_2:Dy^{3+} and ZrO_2:Dy^{3+}, Gd^{3+} films were deposited using the Pyrosol deposition technique. The incorporation of Gd^{3+} ions into the ZrO_2:Dy^{3+} (7 at.%) films produced an notable enhancement of the PL and CL emission intensities due to an energy transfer process. The highest PL and CL emission intensity were reached for films deposited at 550 °C and doped with 7 at.% of Dy^{3+} ions in the precursor solution (1.8 at.% according to measurements by EDS) and 1% in the spraying solution of Gd^{3+} ions. All PL and CL spectra presented bands centered at 480, 574 and 655 nm, corresponding to electronic transitions: $^4F_{9/2} \rightarrow {}^6H_{15/2}$, $^4F_{9/2} \rightarrow {}^6H_{13/2}$ and $^4F_{9/2} \rightarrow {}^6H_{11/2}$ owing to Dy^{3+} ions. The excitation spectrum showed an intense broad band centered at 262 nm, associated to CT absorption among O^{2-} ions and Dy^{3+}. Inhibitions of the PL and CL were observed for doping concentrations above 7 at.% of Dy^{3+} ions and 1% of Gd^{3+} ions. Analysis by X-ray diffraction indicated that the films deposited at higher deposition temperatures showed a poly-crystalline structure corresponding to the meta-stable tetragonal phase of ZrO_2. The estimated size of the constituent

crystallites of the studied films was ~30 nm. The SEM micrographs have shown that the films have rough surfaces with globular morphology at high deposition temperatures. The growth rate of the films was a micrometer per minute. The CIE chromaticity diagram exhibited a bluish-white emission (Dy–Gd doped sample) and a yellowish-white emission (Dy doped sample), which indicates the potential of these films for generating white light.

Finally, it should be emphasized the importance of being able to deposit films at relatively low temperatures with the simple and inexpensive Pyrosol technique, with strong luminescent emissions (PL and CL) very close to pure white color.

Acknowledgements

The authors thank Prof. Prashant Patil for the CIE program, to Omar Novelo for SEM images and EDS measurements, to Adriana Tejeda for XRD measurements and the technical support of M. Guerrero, Z. Rivera, C. Flores, R. Reyes and H. Zarco.

References

[1] G. Blasse, B.C. Grabmaier, Luminescent Materials, Springer-Verlag, Heidelberg, 1994.
[2] T. Hase, T. Kano, E. Nakasawa, H. Yamamoto, Phosphors materials for cathode-ray tubes, in: Peter W. Hawkes (Ed.), Advances in Electronics and Electron Physics, vol. 79, Academic Press, London, 1990.
[3] H.R. Chen, J.L. Shi, Y. Yang, Y.S. Li, D.S. Yan, C.S. Shi, Appl. Phys. Lett. 81 (2002) 2761–2763.
[4] H.K. Yueh, B. Cox, J. Nucl. Mater. 323 (2003) 57–67.
[5] J. Li, X.D. Bai, D.L. Zhang, H.Y. Li, Appl. Surf. Sci. 252 (2006) 7436–7441.
[6] A. Emeline, G.V. Kataeva, A.S. Litke, A.V. Rudakova, V.K. Ryabchuk, N. Serpone, Langmuir 14 (1998) 5011–5022.
[7] E. De La Rosa, L.A. Diaz-Torres, P. Salas, R.A. Rodríguez, Opt. Mater. 27 (2005) 1320–1325.
[8] R. Reisfeld, C.K. Jorgensen, in: K.A. Gschneider, L. Eyring (Eds.), Handbook on the Physics and Chemistry of Rare Earths, vol. 9, Elsevier, Amsterdam, 1987.
[9] M. García-Hipólito, E. Martínez, O. Álvarez-Fregoso, C. Falcony, M.A. Aguilar-Frutis, J. Mater. Sci. Lett. 20 (2001) 1799–1801.
[10] M.R.N. Soares, C. Nico, D. Oliveira, M. Peres, L. Rino, A.J.S. Fernandes, T. Monteiro, F.M. Costa, Mater. Sci. Eng., B 177 (2012) 712–716.
[11] M. García-Hipólito, R. Martínez, O. Álvarez-Fregoso, E. Martínez, C. Falcony, J. Lumin. 93 (2001) 9–15.
[12] B. Marí, K.C. Singh, M. Sahal, S.P. Khatkar, V.B. Taxak, M. Kumar, J. Lumin. 130 (2010) 2128–2132.
[13] F. Ramos-Brito, M. García-Hipólito, C. Alejo-Armenta, O. Alvarez-Fragoso, C. Falcony, J. Phys. D: Appl. Phys. 40 (2007) 6718–6724.
[14] J. Isasi-Marín, M. Pérez-Estébanez, C. Díaz-Guerra, J.F. Castillo, V. Correcher, M.R. Cuervo-Rodríguez, J. Phys. D: Appl. Phys. 42 (2009) 075418 (7pp).
[15] E. De la Rosa-Cruz, L.A. Diaz-Torres, P. Salas, R.A. Rodriguez, G.A. Kumar, M.A. Meneses, J.F. Mosino, J.M. Hernandez, O. Barbosa-Garcia, J. Appl. Phys. 94 (2003) 3509–3515.
[16] A. Martínez-Hernández, J. Guzmán-Mendoza, T. Rivera-Montalvo, D. Sánchez-Guzmán, J.C. Guzmán-Olguín, M. García-Hipólito, C. Falcony, J. Lumin. 153 (2014) 140–143.
[17] Xixin Wang, Jianling Zhao, Peng Du, Limin Guo, Xuewen Xu, Chengchun Tang, Mater. Res. Bull. 47 (2012) 3916–3919.
[18] Z. Assefa, R.G. Haire, P.E. Raison, Spectrochim. Acta Part A Mol. Biomol. Spectrosc. 60 (2004) 89–95.
[19] Feng Gu, Shu Fen Wang, Meng Kai Lu, Guang Jun Zhou, Su Wen Liu, Dong Xu, Duo Rong Yuan, Chem. Phys. Lett. 380 (2003) 185–189.
[20] L.A. Diaz-Torres, E. De la Rosa, P. Salas, V.H. Romero, C. Angeles-Chávez, J. Solid State Chem. 181 (2008) 75–80.
[21] Xiaoyan Fu, Shuyun Niu, Hongwu Zhang, Qin Xin, Mater. Sci. Eng., B 129 (2006) 14–17.
[22] G.A. Hirata, J. McKittrick, M. Avalos-Borja, J.M. Siqueiros, D. Devlin, Appl. Surf. Sci. 113 (114) (1997) 509–514.
[23] L.D. Huy, P. Laffez, Ph. Daniel, A. Jouanneaux, N.T. Khoi, D. Simeone, Mater. Sci. Eng., B 104 (2003) 163–168.
[24] E. Pereyra-Perea, M.R. Estrada-Yáñez, M. García, J. Phys. D: Appl. Phys. 31 (1998) L7–L10.
[25] R. Thomas, A. Milanov, R. Bhakta, U. Patil, M. Winter, P. Ehrhart, R. Waser, A. Devi, Chem. Vap. Deposition 12 (2006) 295–300.
[26] D.M. Hausmann, R.G. Gordon, J. Cryst. Growth 249 (2003) 251–261.
[27] K. Kuratani, M. Mizuhata, A. Kajinami, S. Deki, J. Alloys Compd. 408 (412) (2006) 711–716.
[28] M. Langlet, J.C. Joubert, in: C.N.R. Rao (Ed.), Chemistry of Advanced Materials, Blackwell, Oxford, 1993.
[29] L. Ozawa, Cathodoluminescence. Theory and Applications, Kodansha-VCH Verlag, Germany, 1990.
[30] K. Mishra, S.K. Singh, A.K. Singh, S.B. Rai, Mater. Res. Bull. 47 (2012) 1339–1344.
[31] Hua Lai, Amurisana Bao, Yuming Yang, Weiwei Xu, Yanchun Tao, Hua Yang, J. Lumin. 128 (2008) 521–524.
[32] J.G.C. Bunzli, G.R. Choppin, Lanthanide Probes in Life, Chemical and Earth Sciences; Theory and Practices, Elsevier, Amsterdam, 1989 (Chapter 7).
[33] B.G. Yacobi, D.B. Holt, Cathodoluminescence Microscopy of Inorganic Solids, Plenum, New York, 1990.
[34] L. Robindro Singh, R.S. Ningthoujam, N. Shanta Singh, S. Dorendrajit Singh, Opt. Mater. 32 (2009) 286–292.
[35] Mengistie L. Debasu, Duarte Ananias, Joao Rocha, Oscar L. Malta, Luís D. Carlos, Phys. Chem. Chem. Phys. 15 (2013) 15565–15571.
[36] B.P. Singh, A.K. Parchur, R.S. Ningthoujam, A.A. Ansari, P. Singh, S.B. Rai, Dalton Trans. 43 (2014) 4779–4789.
[37] Anna M. Kaczmarek, Kristof Van Hecke, Rik Van Deun, Inorg. Chem. 53 (2014) 9498–9508.
[38] Y.-C. Li, Y.-H. Chang, Y.-S. Chang, Y.-J. Lin, C.H. Laing, J. Phys. Chem. C 111 (2007) 10682–10688.
[39] Y. Pan, M. Wu, Q. Su, J. Phys. Chem. Solids 65 (2004) 845–850.